



# Non-traditional fractionation of non-traditional isotopes: Evaporation, chemical diffusion and Soret diffusion

Frank M. Richter<sup>a,\*</sup>, Nicolas Dauphas<sup>a,b</sup>, Fang-Zhen Teng<sup>a,1</sup>

<sup>a</sup> The University of Chicago, Department of the Geophysical Sciences, 5734 South Ellis Avenue, Chicago, IL 60637, United States

<sup>b</sup> The University of Chicago, Enrico Fermi Institute, 5640 South Ellis Avenue, Chicago, IL 60637, United States

## ARTICLE INFO

### Article history:

Accepted 5 June 2008

### Keywords:

Isotope fractionation  
Evaporation  
Chemical diffusion  
Thermal diffusion  
Grain boundary diffusion

## ABSTRACT

Recent developments documenting high temperature isotope fractionations of a variety of elements (Li, Mg, Si, Ca, Fe, Ni) by a variety of processes (evaporation, chemical diffusion and thermal diffusion) are reviewed along with some recent applications of these fractionations to Earth and meteoritic problems.

© 2008 Elsevier B.V. All rights reserved.

## 1. Introduction

The study and application of stable isotope fractionations has a long and distinguished history in chemical geology. An important reason for this is that equilibrium fractionations are temperature dependent and thus can be used as geothermometers. Theoretical studies suggested that the magnitude of equilibrium isotopic fractionation decreases as the temperature increases (Bigeleisen and Mayer, 1947; Urey, 1947) and is likely to be negligible during high-*T* processes. Recent high-precision isotope measurements of laboratory and field samples confirm this and show that equilibrium isotopic fractionation of Li and Mg during high temperature magmatic processes is insignificant ( $\leq 0.1\%$  for Mg,  $\leq 1.0$  for Li, Fig. 1) compared to the kinetic and Soret fractionations we discuss in the later sections. For example, little isotopic fractionation is found to have occurred during high temperature crystal–melt differentiation, be it in basaltic (Mg and Li) (Tomascak et al., 1999; Teng et al., 2007), granitic (Li) (Teng et al., 2004; 2006b), peralkaline (Li) (Marks et al., 2007) or carbonatite (Li) (Halama et al., 2007) system. In contrast, Fe isotopes have been found to fractionate by a small but resolvable amount during the differentiation of Kilauea Iki lava. Iron isotopic compositions increase with basaltic differentiation, with olivine cumulates having higher MgO contents, lower  $\delta^{56}\text{Fe}$  and  $\text{Fe}^{3+}/\text{Fe}_{\text{total}}$  ratios while late-stage veins have lower MgO contents, higher  $\delta^{56}\text{Fe}$  and  $\text{Fe}^{3+}/\text{Fe}_{\text{total}}$  ratios

(Teng et al., 2008a). This  $> 0.2\%$  Fe isotopic variation is interpreted to be caused by fractional crystallization, with an estimated isotopic fractionation between minerals and melts of  $\sim -0.1\%$ . The fractionation of Fe isotopes at high temperature could be produced by kinetic or equilibrium effects and may be associated with the changing oxidation state of Fe.

The smallness of the expected and observed equilibrium isotope fractionations at high temperature resulted in an unwarranted tendency to ignore high temperature isotope fractionation processes. But this is changing, in part because of the increasing precision of modern isotopic measurements that allow for even small degrees of fractionation to be resolved. Another reason is that once higher temperature non-equilibrium isotope fractionations began to be explored, surprisingly large effects were often found.

In the following sections we selectively review some recent developments in the emerging field of high temperature isotope fractionation. We should make clear that our purpose is to be illustrative rather than comprehensive in our review of different types of high temperature fractionation process involving evaporation, chemical diffusion, and thermal (i.e., Soret) diffusion. We will draw quite heavily on some of our own recent work, but the lack of extensive references to other works should not be taken to imply that these do not exist or that given that they do exist, that they are not worthwhile.

The experiments we review to illustrate kinetic isotope fractionation during evaporation involve silicon and magnesium and iron, which are among the more volatile components of a silicate melt. The motivation for the evaporation studies comes from the observation that certain components in primitive meteorites have heavy isotopic compositions for the more volatile species. The sections on isotope fractionation by chemical diffusion discuss effects in molten rhyolite-

\* Corresponding author.

E-mail address: [richter@geosci.uchicago.edu](mailto:richter@geosci.uchicago.edu) (F.M. Richter).

<sup>1</sup> Present address: Department of Geosciences and Arkansas Center for Space and Planetary Sciences, The University of Arkansas, Fayetteville, AR 72701, United States.

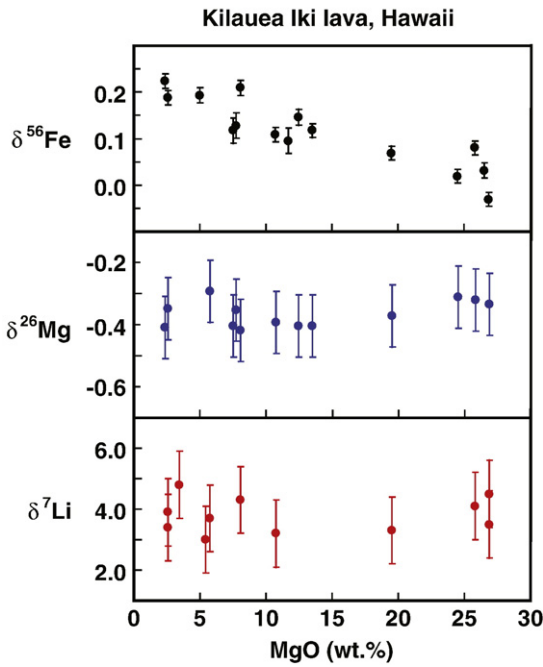


**Fig. 1.**  $^{56}\text{Fe}/^{54}\text{Fe}$  (Teng et al., 2008a),  $^{26}\text{Mg}/^{24}\text{Mg}$  (Teng et al., 2007) and  $^7\text{Li}/^6\text{Li}$  (Tomascak et al., 1999) of samples from the Kilauea Iki lava lake (Hawaii) as a function of the weight percent MgO, which decreases with increasing crystallization (Helz, 1987). A change in isotopic composition with wt.% MgO would indicate a crystal–melt isotopic fractionation. The isotopic composition is reported using standard delta notation for the isotope ratio  $^{m}X/^{n}X$ .

$$\delta^mX(\%) = 1000 \times \left[ \left( \frac{^{m}X/^{n}X}{^{m}X/^{n}X}_{\text{standard}} \right) - 1 \right].$$

basalt, in iron–nickel alloys, and in grain boundaries. The study of diffusive fractionations in metal systems is motivated by some recent measurements of iron and nickel isotope fractionations in iron meteorites. Isotope fractionation by grain boundary diffusion is the most likely explanation for the very large isotopic fractionations of lithium that migrated from a pegmatite into a surrounding amphibolite. The final example we discuss of high temperature isotopic fractionations involves thermal (i.e., Soret) diffusion of an initially homogeneous molten natural mid-ocean ridge basalt. The distinctive feature of thermal isotope fractionations is that they result in a steady state separation that persists as long as the temperature difference is maintained. In a closing section we consider some implications and potential applications of high temperature isotope fractionations for chemical geology.

## 2. Isotope fractionation by evaporation at high temperatures

The motivation to study the elemental and isotopic fractionations associated with evaporation from molten silicate liquids comes from the observation that certain components of primitive meteorites – calcium aluminum-rich refractory inclusions (CAIs) – have correlated enrichments in the heavy isotopes of silicon and magnesium (see discussion and Fig. 1 in Davis and Richter, 2004). As we show below, this correlation of silicon and magnesium isotopic fractionations is typical of silicate evaporation residues.

The standard representation for the net evaporation or condensation flux of an element or isotope  $i$  between a condensed phase and a surrounding gas is the Hertz–Knudsen equation (see Hirth and Pound, 1963)

$$J_i = \frac{n_i \gamma_i (P_{i,\text{sat}} - P_i)}{\sqrt{2\pi m_i RT}} \quad (1)$$

For the silicate liquids we discuss here, the gas is dominated by a single species containing  $i$  (i.e., silicon as SiO, magnesium as Mg).  $J_i$  is

the net flux of  $i$  in moles per unit area per unit time,  $n_i$  is the number of atoms of  $i$  in the gas species molecule,  $\gamma_i$  is a condensation coefficient,  $P_{i,\text{sat}}$  is the saturation vapor pressure of  $i$ ,  $P_i$  is the pressure of  $i$  at the evaporating surface,  $m_i$  is the molar mass of gas species containing  $i$ ,  $R$  is the gas constant, and  $T$  is absolute temperature. This representation derives from the kinetic theory of ideal gases where  $P_i/\sqrt{2\pi m_i RT}$  is the rate of collision with the surface of the species containing  $i$ . If only a fraction  $\gamma_i$  of the molecules impinging on the surface stick (i.e., condense), then the condensation flux of  $i$  will be reduced by this factor  $\gamma_i$ . At equilibrium,  $P_i = P_{i,\text{sat}}$  and there is no net flux of  $i$  from the condensed phase, thus an evaporation flux proportional to  $\gamma_i P_{i,\text{sat}}$  must balance the condensation flux. Eq.(1) implies that the evaporation will remain proportional to  $\gamma_i P_{i,\text{sat}}$  for all values of  $P_i$  including zero (i.e., whether or not there is recondensation).

The kinetic isotope fractionation experiments we discuss in this section involve the evaporation of silicon and magnesium from a silicate liquid into vacuum ( $P_i \rightarrow 0$ ). Laboratory experiments and thermodynamic calculations of gas speciation (Nichols et al., 1998) show that the dominant gas species that would be in equilibrium with a CaO–MgO–Al<sub>2</sub>O<sub>3</sub>–SiO<sub>2</sub> liquid are Mg and SiO, thus  $n_i = 1$ . Eq.(1) becomes

$$J_i = \frac{\gamma_i P_{i,\text{sat}}}{\sqrt{2\pi m_i RT}} \quad (2)$$

which can be used to write the isotopic ratio of the evaporation flux as

$$\frac{J_i}{J_j} = \frac{\gamma_i P_{i,\text{sat}}}{\gamma_j P_{j,\text{sat}}} \sqrt{\frac{m_j}{m_i}} \quad (3)$$

The expectation that evaporation will fractionate isotopes derives from the square root of the ratio of the atomic mass of the dominant gas species in Eq. (3). The usual practice is to define a fractionation factor  $\alpha_{ij}$  corresponding to the ratio of the fluxes of individual isotopes,  $J_i/J_j$ , divided by the atom ratio of the isotopes in the condensed phase,  $N_i/N_j$ . When, as is the case here, equilibrium isotopic fractionations are negligible (i.e.,  $P_{i,\text{sat}}/P_{j,\text{sat}} = N_i/N_j$ ), the kinetic isotope fractionation factor becomes  $\alpha_{ij} = (\gamma_i/\gamma_j) \sqrt{m_j/m_i}$ . It has often been assumed that the kinetic fractionation factor is simply proportional to the inverse square root of the mass of the isotopologues of the gas species, implying that  $\gamma_i = \gamma_j$ . This, as we show below, is demonstrably incorrect in many cases, and therefore laboratory experiments remain essential for determining how isotopes fractionate during evaporation.

Another common assumption is that evaporation residues will become isotopically fractionated in a manner referred to as Rayleigh fractionation, which is governed by an equation of the form

$$\frac{R_{ij}}{R_{ij,0}} = f_j^{\alpha_{ij}-1} \quad (4)$$

where  $R_{ij,0}$  is the isotopic ratio  $N_i/N_j$  of isotopes  $i$  and  $j$  in the condensed phase prior to evaporation,  $R_{ij}$  is the isotopic ratio of the evaporation residue when a fraction  $f_j$  of isotope  $j$  remains, and  $\alpha_{ij}$  is the kinetic isotope fractionation factor defined above. A derivation and discussion of the conditions when Eq (4) can be used for evaporation residues (mainly  $P_i \ll P_{i,\text{sat}}$  and  $\alpha_{ij}$  unchanging as evaporation proceeds) is given in Richter (2004). Rayleigh fractionation of evaporation residues can be tested by plotting the measured isotopic and elemental fractionations as  $\ln(R_{ij}/R_{ij,0})$  versus  $-\ln f_j$ . According to Eq. (4), Rayleigh fractionation will result in the data plotting along a line of slope  $1 - \alpha_{ij}$ .

### 2.1. Experimental results

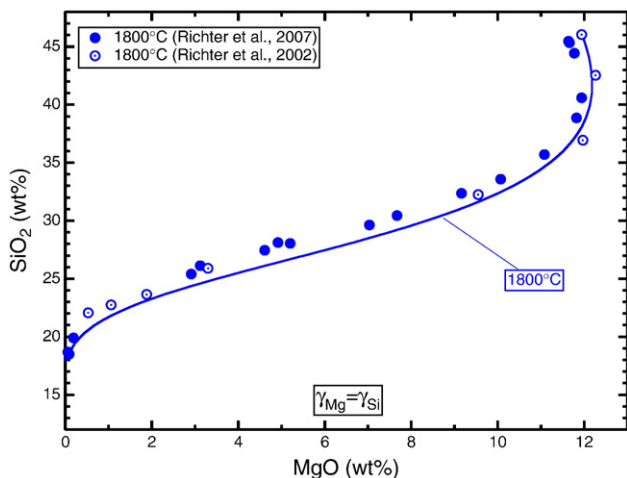
High-precision isotopic fractionation measurements of vacuum evaporation residues have a relatively short history dating back to the classic paper by Davis et al. (1990) reporting Rayleigh-like isotopic

fractionations of silicon, magnesium, and oxygen associated with vacuum evaporation of molten forsterite ( $\text{Mg}_2\text{SiO}_4$ ). Here we review recent experimental results directly relevant to the interpretation of Type B CAIs in primitive meteorites as evaporation residues. These CAIs are especially interesting because they are the oldest known objects to have formed in the protoplanetary disk around our Sun. They are often found to be enriched in the heavier isotopes of silicon and magnesium.

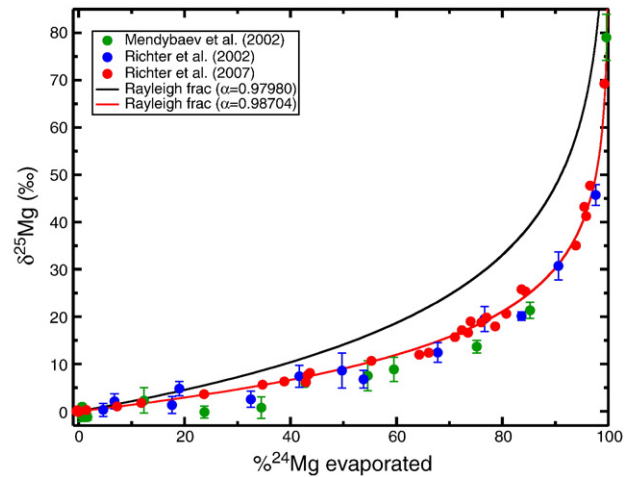
The starting materials for the evaporation experiments motivated by the Type B CAIs were prepared by mixing appropriate amounts of high-purity (> 99.99%)  $\text{SiO}_2$ ,  $\text{Al}_2\text{O}_3$ ,  $\text{MgO}$ , and  $\text{CaCO}_3$ , which when decarbonated, produced starting material with approximately 11.5wt.%  $\text{MgO}$ , 46.0wt.%  $\text{SiO}_2$ , 19.5wt.%  $\text{Al}_2\text{O}_3$  and 23.0wt.%  $\text{CaO}$ . A small amount (4–200 mg) of the starting material was loaded onto iridium wire loops that were then suspended in a high temperature vacuum furnace at the University of Chicago designed and constructed by A. Hashimoto (see Hashimoto, 1990). The run conditions involved temperatures from 1600 °C to 1900 °C with a pressure outside the heating elements and heat shields surrounding the sample of less than  $10^{-6}$  Torr. The major element composition of the starting materials and chips of the evaporation residues were measured using a JEOL JSM-5800LV scanning electron microscope (SEM) with an Oxford Link ISIS-300 energy dispersive microanalysis system (EDS). The magnesium isotopic composition of the starting materials and of the evaporation residues was measured on dissolved and purified solutions using a CETAC Aridus desolvating nebulizer as input to a Micromass Isoprobe multi-collector magnetic sector inductively coupled plasma mass spectrometer (MC-ICPMS). Details regarding the magnesium isotopic measurements are reported in Richter et al. (2007). The silicon isotopic composition of the starting materials and selected evaporation residues was measured using a eximer laser ablation system (New Wave Research 193HE) to introduce material into the Micromass Isoprobe MC-ICPMS. For details regarding the silicon isotopic measurements see Janney et al. (2005).

Fig. 2 shows the trajectory in  $\text{SiO}_2$ – $\text{MgO}$  space of a set of vacuum evaporation residues that were evaporated at 1800 °C for various lengths of time. The  $\text{CaO}$  and  $\text{Al}_2\text{O}_3$  components are sufficiently refractory that they were not measurably evaporated.

Fig. 3 shows the heavy magnesium isotope enrichment of evaporation residues as a function of the fraction of magnesium evaporated for vacuum experiments run at temperatures between 1600 °C and 1900 °C.



**Fig. 2.** Weight percent  $\text{SiO}_2$  and  $\text{MgO}$  of vacuum evaporation residues of molten  $\text{CaO}$ – $\text{MgO}$ – $\text{Al}_2\text{O}_3$ – $\text{SiO}_2$  held for various lengths of time at 1800 °C. The  $\text{CaO}$  and  $\text{Al}_2\text{O}_3$  components are sufficiently refractory that they were not measurably reduced by evaporation. The curve is an evaporation trajectory as calculated using Eq. (2) with a thermodynamic model to calculate the saturation vapor pressures of  $\text{SiO}$  and  $\text{Mg}$  and assuming that the evaporation coefficients for  $\text{Si}$  and  $\text{Mg}$  are the same. Figure taken from Richter et al. (2007).



**Fig. 3.** Magnesium isotopic fractionation of vacuum evaporation residues relative to the starting material as a function of the %  $^{24}\text{Mg}$  evaporated from molten  $\text{CaO}$ – $\text{MgO}$ – $\text{Al}_2\text{O}_3$ – $\text{SiO}_2$  at temperature ranging from 1600 °C to 1900 °C. Rayleigh fractionation curves for two choices of the kinetic isotope fractionation factor  $\alpha$  for magnesium are also shown. Figure taken from Richter et al. (2007).

The test of whether or not the isotopic fractionations of evaporation residues obey a Rayleigh fractionation rule involves plotting the data as  $\ln(R_{ij}/R_{ij,0})$  against  $-\ln(f_j)$ . According to Eq. (4), the data plotted in this fashion will, if they correspond to Rayleigh fractionation, fall on a line of slope  $1 - \alpha_{ij}$ . Fig. 4 uses this approach to show that the magnesium isotopic fractionation of vacuum evaporation residues run at a particular temperature is a form of Rayleigh fractionation. The data for residues evaporated at different temperatures are sufficiently precise to resolve a slight temperature dependence of the kinetic isotope fractionation factor for magnesium evaporating from a CAI-like liquid. This temperature dependence needs to be taken into account when using the kinetic isotope fractionation factor to interpret the isotopic composition of actual CAIs because these were most likely evaporated at temperatures not much higher than 1400 °C (see Stolper and Paque, 1986 for a discussion of peak temperatures experienced by the CAIs). Additionally, Richter et al. (2007) evaporated samples that differed in size by a factor of six and showed that there was negligible effect of size on the measured kinetic isotope

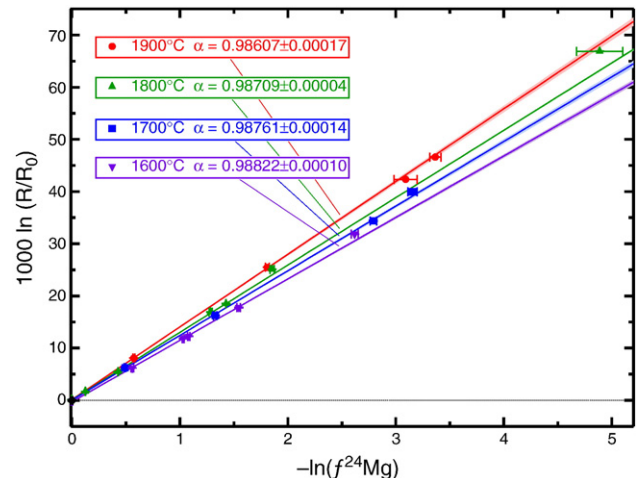


**Fig. 4.** Isotopic fractionation of vacuum evaporation residues from molten CAI-like starting compositions run at various temperatures. Results are plotted such that fractionations derived from a Rayleigh fractionation process would plot on a line of slope  $1 - \alpha$  where  $\alpha$  corresponds to the kinetic fractionation factor  $\alpha_{ij}$  for  $^{25}\text{Mg}$  and  $^{24}\text{Mg}$  defined in the text.  $R$  is the  $^{25}\text{Mg}/^{24}\text{Mg}$  of a residue sample,  $R_0$  is the  $^{25}\text{Mg}/^{24}\text{Mg}$  of the starting composition and  $f^{24}\text{Mg}$  is the fraction of the original  $^{24}\text{Mg}$  remaining in the residue. Figure taken from Richter et al. (2007).

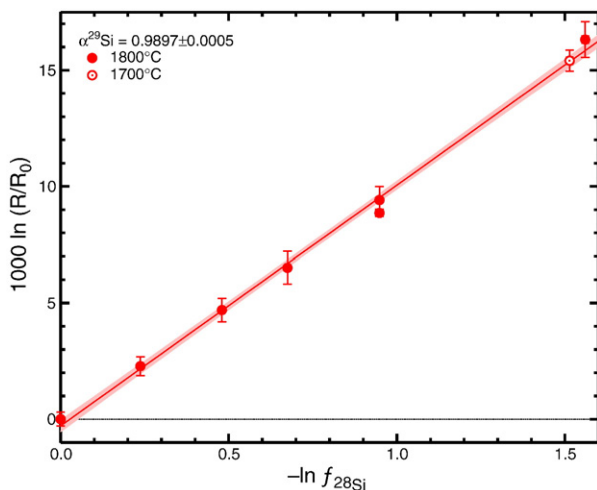
fractionation of the evaporation residues. From this they concluded that the results were not affected by recondensation or by diffusion in the evaporating liquid drop since, if important, these would have affected the larger samples more than the smaller ones.

Fig. 5 shows the silicon isotopic fractionation of a set of residues evaporated into vacuum at 1800 °C and one sample evaporated at 1700 °C. The data fall on a straight line indicating Rayleigh fractionation with the slope of the line corresponding to  $1-\alpha$  where  $\alpha$  is the kinetic isotope fractionation factor for  $^{29}\text{Si}/^{28}\text{Si}$ .

## 2.2. Discussion

As noted earlier, it has often been assumed that the kinetic fractionation factor  $\alpha_{ij}$  is equal to the inverse square root of the mass of the isotopologues of the gas species (i.e.,  $\alpha_{ij} = (m_j/m_i)^{1/2}$ ). This is certainly not the case for either silicon or magnesium in evaporation residues of Type B CAI-like composition where as noted above the relevant gas species are Mg and SiO. It follows that the evaporation coefficients of isotopes must in at least some cases be mass dependent (i.e.,  $\gamma_i/\gamma_j \neq 1$ ). The case of iron isotopic fractionations in evaporation residues is particularly interesting in that when iron evaporates from molten FeO, the kinetic isotope fractionation factor for  $^{56}\text{Fe}/^{54}\text{Fe}$  (the dominant gas species being Fe) was found to be equal to  $(54/56)^{1/2}$ , but significantly different from this when FeO evaporates from a silicate liquid (Dauphas et al., 2004). There appears to be no simple way of predicting the kinetic isotope fractionation factor for species evaporating from molten silicate liquids, and therefore laboratory experiments remain an essential tool for interpreting evaporation residues.

The primary motivation for our experiments aimed at determining the kinetic isotope fractionation of silicon and magnesium of evaporation residues derives from the observation noted earlier that the Type B CAIs are often enriched in the heavy isotopes of these two elements. The correlated isotopic fractionation of silicon and magnesium seen in laboratory evaporation residues is sufficiently like that of the actual CAIs to make a very strong case that many CAIs were similarly affected by evaporation of a significant fraction of their initial silicon and magnesium. Once one accepts this conclusion one can use the isotopic fractionation of CAIs to determine the fraction of silicon and magnesium that must have been volatilized to account for their isotopic composition, which in turn can be combined with laboratory determinations of the evaporation rate as a function of temperature and surrounding gas pressure to constrain the thermal history of these earliest materials to



**Fig. 5.** Silicon isotopic fractionation of vacuum evaporation residues of molten CAI-like liquids run at 1800 °C, and one run at 1700 °C, plotted against  $-\ln f_{28\text{Si}}$ , where  $f_{28\text{Si}}$  is the fraction of  $^{28}\text{Si}$  remaining in the residue.  $R$  is the  $^{29}\text{Si}/^{28}\text{Si}$  of a residue sample,  $R_0$  is the  $^{29}\text{Si}/^{28}\text{Si}$  of the starting composition. The slope of the line defined by the data corresponds to a kinetic isotope fractionation factor  $\alpha = 0.9898$ . Data taken from Janney et al. (2005) with additional subsequent measurements.

have formed in our solar system (see Richter et al. (2006a) for a detailed example of this approach for the thermal history of the Type B CAIs).

Experimental evidence for isotopic fractionation associated with condensation is missing but zoned metal grains found in several chondrite groups are examples that it does occur in nature. Measurements available have revealed very large and correlated fractionations in these grains, with the cores having light Fe and Ni isotopic compositions relative to the rims (down to  $-8\text{‰}$ amu; Alexander and Hewins, 2004; Zipfel and Weyer, 2007). The extent of the isotopic fractionations can only be explained by condensation.

## 3. Isotope fractionation by chemical diffusion

Some of the clearest examples of the large isotopic fractionations that can arise during chemical diffusion involve lithium. It has been known for some time that the large ratio of mass between  $^6\text{Li}$  and  $^7\text{Li}$  can give rise to significant isotopic fractionation at low temperatures as is the case for water–rock interactions (e.g., Chan et al., 1992) and weathering (e.g., Rudnick et al., 2004). Similarly large fractionations at high temperature were not generally expected. However, recent studies using both laboratory experiments and natural rocks have demonstrated exceptionally large isotopic fractionation at high temperature, due to the significantly faster (up to 3%) diffusivity of  $^6\text{Li}$  relative to  $^7\text{Li}$  in melts, minerals and rocks (Richter et al., 2003; Lundstrom et al., 2005; Beck et al., 2006; Teng et al., 2006a; 2008b; Jeffcoate et al., 2007; Marks et al., 2007; Rudnick and Ionov, 2007; Tang et al., 2007; Aulbach et al., 2008).

### 3.1. Isotope fractionation by diffusion in a silicate melt

The first laboratory study that clearly showed large diffusive fractionations of Li isotopes ( $\sim 40\text{‰}$ ) at high temperature ( $T = 1350\text{ °C}$ ) was done by Richter et al. (2003). A diffusion couple juxtaposing basalt (doped with spodumene to increase the lithium concentration to about 800 ppm) and rhyolite (about 20 ppm Li) was annealed in a piston cylinder apparatus at 1350 °C and 1.2 GPa for only 6 min. The Li profile that developed over 6 min was shown by Richter et al. (2003) to be consistent with diffusion profiles developed in longer duration runs by comparing profiles normalized by the square root of time. The very short duration of the experiment was required because of the extraordinarily fast diffusion of lithium compared to all other components in the melt. The lithium isotopic fractionation was generated by the lighter isotope ( $^6\text{Li}$ ) diffusing measurably faster than the heavier isotope ( $^7\text{Li}$ ). The basalt side of the couple lost  $^6\text{Li}$  faster than  $^7\text{Li}$  and as a result became isotopically heavy while the rhyolite became preferentially enriched in  $^6\text{Li}$  and thus isotopically light. Fig. 6 taken from Richter et al. (2003) shows the isotopic variation of about 40‰ produced by the diffusion of lithium from the basalt into the rhyolite. Richter et al. (2003) fit the lithium elemental and isotopic data shown in Fig. 6 using a simple chemical diffusion model in which the ratio of the diffusivity  $D_6$  and  $D_7$  of  $^6\text{Li}$  and  $^7\text{Li}$  depends on their mass as  $D_6/D_7 = (7/6)^\beta$  with  $\beta = 0.215$ , (i.e.,  $^6\text{Li}$  diffuses  $\sim 3\%$  faster than  $^7\text{Li}$  in the silicate melts).

Isotope fractionation by chemical diffusion in a silicate melt is not restricted to lithium. Richter et al. (1999, 2003) showed that calcium isotopes were measurably fractionated by diffusion in silicate liquids and Richter et al. (2008) showed that magnesium isotopes were similarly fractionated by diffusion between basalt and rhyolite. Our most recent as yet unpublished experiments show that iron isotopes are also fractionated by diffusion between basalt and rhyolite, but to a somewhat lesser degree than the calcium or magnesium isotopes. Richter et al. (1999) reported no measurable isotopic fractionation of germanium isotopes diffusing in molten  $\text{GeO}_2$ . To the extent that germanium is often used as an analogue for silicon (to avoid the very high melting temperature of  $\text{SiO}_2$ ) the germanium result suggests that silicon isotopes are not significantly fractionated by diffusion.

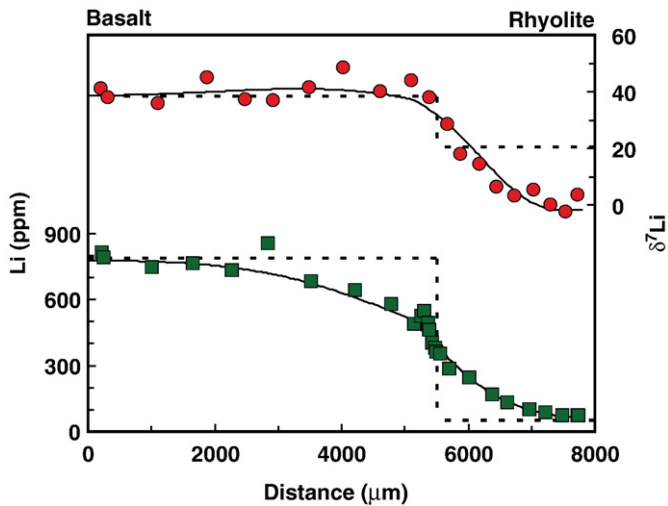


**Fig. 6.** Lower panel: Lithium concentration as a function of distance in a diffusion couple made of lithium-doped basalt on the left and rhyolite on the right that had been annealed for 6 min at 1350 °C in a piston cylinder apparatus ( $P = 1.2\text{GPa}$ ). The dashed lines indicate the starting distribution of lithium. The solid curve is a model fit based on a diffusion model with different diffusion coefficients for lithium in the silica-rich rhyolite (72wt.%  $\text{SiO}_2$ ) and in the silica-poor basalt (50wt.%  $\text{SiO}_2$ ). Upper panel: Lithium isotopic composition in per mil as a function of distance. The dashed lines show the initial isotopic composition while the solid curve shows the fit to the isotopic data using  $D_7 / D_6 = (m_6 / m_7)^\beta$  with  $\beta = 0.215$ . Figure taken from Richter et al. (2003). There is initially so little Li in the rhyolite side compared to what diffuses in that the initial Li isotopic composition of the rhyolite has little effect on the final isotopic fractionations seen in the data or in the calculated profile.

### 3.2. Isotope fractionation by grain boundary diffusion

A natural example of diffusion-driven isotopic fractionation was recently found in country rocks of the Tin Mountain pegmatite, Black Hills, South Dakota (Teng et al., 2006a). The Li-rich Tin Mountain pegmatite discordantly intruded both schists and a tabular amphibolite unit at ~ 10 km depth at about 1.7Ga (Walker et al., 1986). This pegmatite body is extremely enriched in isotopically heavy Li relative to the adjacent amphibolite and schist country rocks. Consequently, the large Li concentration contrast led to diffusion of Li from the pegmatite into both country rocks. The amphibolite adjacent to the pegmatite has high Li concentration (up to 470 ppm) and  $\delta^7\text{Li}$  similar to that of the pegmatite (~ + 8‰). Both Li concentration and  $\delta^7\text{Li}$  fall systematically from this contact, with  $\delta^7\text{Li}$  reaching a low of - 20‰ at a distance of 10 m from the pegmatite, where the outcrop ends (Fig. 7). The Li concentration is still relatively high at this distance (70 ppm). It is assumed that beyond 10 m the Li concentration will continue to fall back to values unaffected by diffused lithium, approaching the regional amphibolite Li content (20 ppm) and that  $\delta^7\text{Li}$  will increase to the regional value of + 1‰. The lithium diffusion profile in the schists is similar but not as well constrained as in the amphibolite due to more limited sampling access.

The data shown in Fig. 7 cannot be explained as being due to mixing because of the extreme end-member  $\delta^7\text{Li}$  value that would be required for mixing (< - 20‰). Teng et al. (2006a) have argued that the most likely explanation is diffusion-driven kinetic isotopic fractionation at temperatures of 340 °C–600 °C. Teng et al. (2006a) modeled the lithium isotopic data and found that the data could be fit assuming that the ratio of the diffusivity between  $^6\text{Li}$  and  $^7\text{Li}$  is related to their mass by  $D_6 / D_7 = (m_7 / m_6)^\beta$ , with  $\beta = 0.12$ . This value of  $\beta$  is smaller than that in silicate melt (Richter et al., 2003) but much larger than that measured in water (Richter et al., 2006b). The inferred diffusion coefficient for Li in the amphibolite is significantly greater than that in the constituent minerals (Coogan et al., 2005; Giletti and Shanahan, 1997), implying that Li was primarily diffusing through grain boundaries rather than through the minerals. In addition, as was

found for melts, Li diffuses far faster than all other mobile elements that were measured (e.g., Rb, Cs, Na, Sb), which show enrichments only within 2 m of the contact.

### 3.3. Isotope fractionation by volume diffusion in metals

In contrast to the situation for isotope fractionations by diffusion in silicate liquids or in grain boundaries, there is a very extensive literature on such effects in metals. In this section, we review experimental constraints on diffusion-driven kinetic isotopic fractionation of metals and metalloids and show how it relates to the petrogenesis of iron meteorites (Dauphas, 2007), which were witnesses to the formation of the solar system and became key building blocks for the Earth. Roskosz et al. (2006) performed an experiment of Fe segregation from a silicate melt into platinum metal at a temperature of 1500°C. They showed that the transfer of iron was limited by diffusion in Pt and found large Fe isotopic fractionation within the Pt loop. They could explain their results by invoking

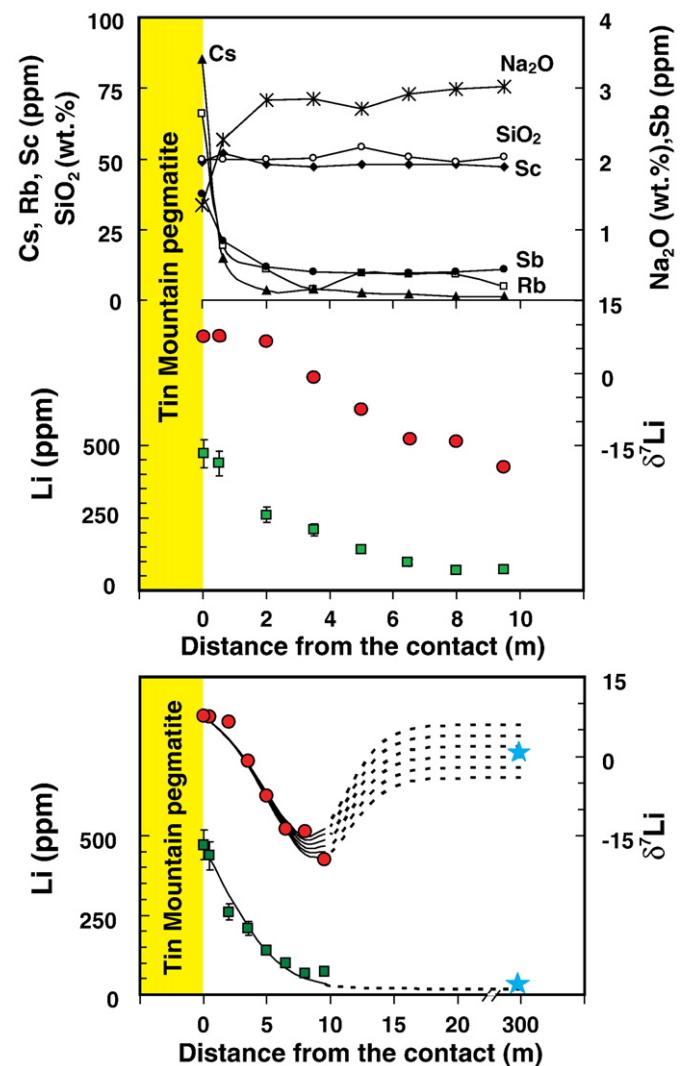


**Fig. 7.** Kinetic Li isotopic fractionation during Li diffusion from Tin Mountain pegmatite to amphibolite country rocks. The top figure shows concentration profiles of fluid-mobile (Rb, Cs, Sb,  $\text{Na}_2\text{O}$ ) and fluid-immobile (Sc and  $\text{SiO}_2$ ) elements as well as Li isotopic profile in the amphibolite country rocks. The lower figure shows the diffusion profiles as well as model curves for a range of concentrations assumed in the amphibolite and for a kinetic isotope fractionation factor  $\beta = 0.12$ . The stars represent the regional amphibolite lithium concentration and isotopic composition measured at 300 m from the pegmatite body, which was not affected by the pegmatite. Modified from Teng et al. (2006a).

**Table 1**  
Kinetic isotope fractionation factors for diffusion in silicate liquids

Element	Fractionation factor $\beta^a$	Reference
Lithium	0.215	Richter et al. (2003)
Calcium	0.05–0.075	Richter et al. (1999, 2003)
Magnesium	0.05	Richter et al. (2008)
Iron (2+)	0.015–0.02	Unpublished data
Germanium	<0.02	Richter et al. (1999)

<sup>a</sup> The fractionation factor  $\beta$  is defined in terms of the experimentally determined relative diffusion coefficients  $D_i$  and  $D_j$  of the isotopes  $i$  and  $j$  of mass  $m_i$  and  $m_j$  parameterized by  $D_i/D_j = (m_j/m_i)^\beta$ .

diffusive separation of Fe isotopes corresponding to  $\beta$  between 0.2 and 0.3 in the usual parameterization of the dependence of the diffusion coefficients  $D_i$  and  $D_j$  of the form  $D_i/D_j = (m_j/m_i)^\beta$  where  $m_i$  and  $m_j$  are the mass of isotopes  $i$  and  $j$ . This range of  $\beta$  values represents a difference between the diffusivities of <sup>54</sup>Fe and <sup>56</sup>Fe of almost 1%. For comparison,  $\beta$  for diffusion of Fe in water at room temperature is estimated to be around 0.002 (Rodushkin et al., 2004) and for diffusion in silicate liquids at 1450 °C,  $\beta$  is estimated to be around 0.02 (Table 1). Thus, diffusion in metals seems to be exceptionally efficient at fractionating isotopes at high temperatures. This has been well documented since around 1960 by material scientists studying the mechanism of diffusion in metals (see references in the caption of Fig. 8).

The typical experimental setup used by physicists, chemists, and material scientists (e.g., Mullen, 1961) for investigating what they refer to as the isotope effect (fractionation) is different from that used by Earth scientists. An example taken from the pioneering study of Mullen (1961) of Fe diffusion in Cu and Ag at 718–1056 °C is typical. Single crystals of Ag and Cu were grown, sectioned into cylinders (1.9 cm diameter and 1.3 cm thick), and finely polished. Radioactive isotopes of iron (<sup>55</sup>Fe and <sup>59</sup>Fe) were plated on the specimens (3 to 10 atom layers). The ends of the specimens were covered with quartz plates to prevent evaporation during heating. The sample assemblies

were annealed to allow diffusion of the radioactive isotopes into the cylinders. After quenching in water, the cylinders were mounted on a precision lathe and 0.25 mm-thick sections were sampled. The isotopic ratios <sup>55</sup>Fe/<sup>59</sup>Fe in each chip were then measured by counting (5.9 keV X-ray for <sup>55</sup>Fe and 1.1 MeV  $\gamma$ -ray for <sup>59</sup>Fe). Fick's law of diffusion can be applied to this simple system and one expects a linear correlation between the isotopic composition and a dimensionless parameter quantifying penetration,

$$\ln \frac{^{55}\text{Fe}}{^{59}\text{Fe}} = \text{constant} + \left(1 - \frac{D_{59}}{D_{55}}\right) \frac{x^2}{4D_{59}t}$$

The slope of this correlation directly gives the ratio of the diffusion coefficients  $1 - D_{59} / D_{55}$ . The isotopic effects measured by Mullen (1961) are very large, reaching ~ 100%. As shown in Fig. 9, measured <sup>55</sup>Fe/<sup>59</sup>Fe ratios plotted as a function of  $x^2/4D_{59}t$  for Fe diffusion in Cu and Ag at ~ 720 °C gives a  $\beta$  of ~ 0.3. An extensive review of the literature on isotopic fractionation associated with diffusion of metals and metalloids shows that  $\beta$  is almost always in the range 0.1 to 0.4 (Fig. 8, also see Fig. 3 of Dauphas, 2007 for Fe). The fractionation factor is not obviously dependent on the temperature, the specific diffusing element, or the diffusion medium (e.g.,  $\beta$  for self-diffusion of Na at – 25.5 °C is 0.195 and  $\beta$  for self-diffusion of Nb at 2400 °C is 0.172; Mundy, 1971; Bussmann et al., 1981).

The differences seen in Fig. 8 are of great interest to physicists, chemists, and material scientists who study the mechanisms of diffusion. During diffusion via the random walk of lattice vacancies, the directions of consecutive jumps are correlated (e.g., after an atom has just jumped to an adjacent vacancy, it is more likely to jump back to its initial position, now a vacancy, than move in other directions). Departure from an Einstein-type random walk is quantified using a correlation factor  $f$  (e.g., LeClaire and Lidiard, 1956). The correlation factor for a given lattice depends on details of the diffusion mechanism (e.g., LeClaire and Lidiard, 1956). In vacancy diffusion, isotopic substitution affects jump frequencies in a predictable manner

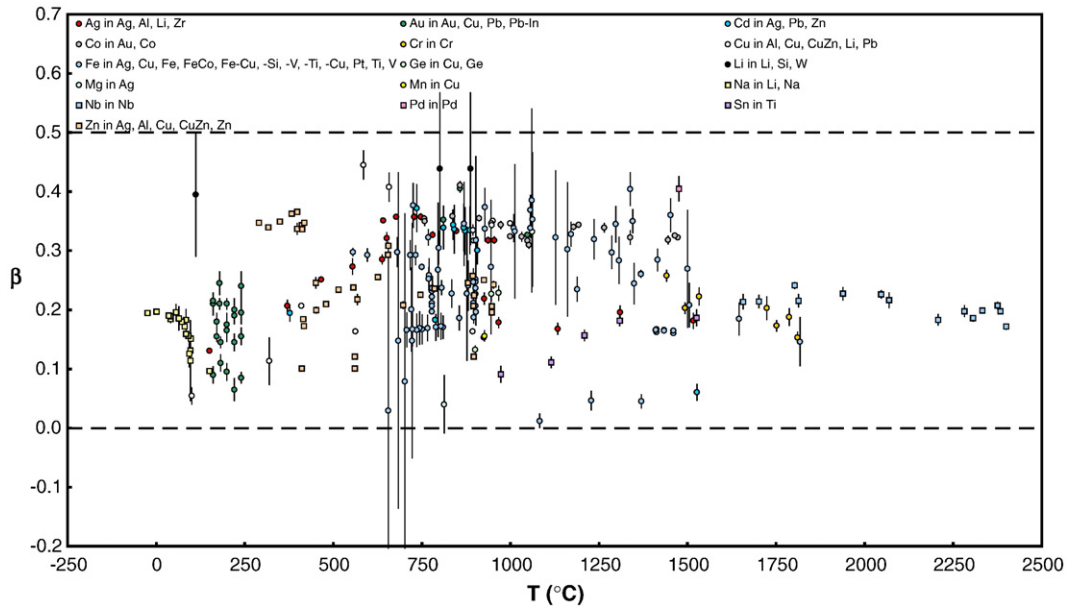


**Fig. 8.** Isotopic fractionation associated with diffusion of metals and metalloids.  $\beta$  parameterizes the mass dependence of diffusion coefficients of isotopes,  $D_2 / D_1 = (m_1 / m_2)^\beta$ . The dashed horizontal lines correspond to no mass dependence ( $\beta = 0$ ) and square root mass dependence ( $\beta = 0.5$ ). As illustrated, for most metals/metalloids and at all temperatures,  $\beta$  is between 0 and 0.4 (McCracken and Love, 1960; Pell, 1960; Mullen, 1961; Gibbs et al., 1963; Peterson, 1964; Batra, 1967; Peterson and Rothman, 1967a, 1967b, 1970, 1978; Rothman and Peterson, 1967; Coleman et al., 1968; Heumann and Imm, 1968; Graham, 1969; Miller and Edelstein, 1969; Tothman and Peterson, 1969; Walter and Peterson, 1969; Fishman et al., 1970; Rothman et al., 1970; Mundy, 1971; Oviedo de Gonzalez and Walsoe de Reca, 1971; Irmer and Feller-Kniepmeier, 1972; Mundy and McFall, 1973; Heumann and Kohl, 1974; Mundy et al., 1974; 1976; Bartdorff and Reimers, 1975; Campbell, 1975; Bharati and Sinha, 1977; Hehenkamp and Schlett, 1977; Jackson and Lazarus, 1977; Eckseler and Herzig, 1978; Herzig et al., 1978; Bussmann et al., 1979, 1981; Hehenkamp et al., 1979; Manke and Herzig, 1982; Rockosch and Herzig, 1983, 1984; Iijima et al., 1988; Mali et al., 1988; Shi et al., 1994; Roskosz et al., 2006).

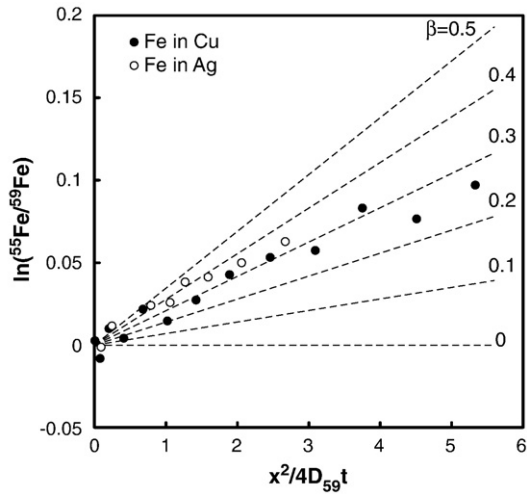


Fig. 9. Example of determination of  $\beta$  for diffusion of Fe in Cu and Ag at  $\sim 720$  °C using radioactive isotope experiments (Mullen, 1961). The slope in this diagram gives  $1 - D_{59}/D_{55}$ , which depends on  $\beta$ .

and can be used to estimate the correlation factor (e.g., Schoen, 1958; Mullen, 1961). For instance, from his experiments, Mullen (1961) could exclude the ring mechanism as being responsible for diffusion of Fe in Cu and Ag because the predicted isotopic fractionation would be smaller than what he observed.

### 3.4. Isotope fractionation in iron meteorites

Our interest in isotopic fractionations by diffusion of metals in metal derives from what such isotopic fractionations can contribute to the determination of metallographic cooling rates of iron meteorites. The Widmanstätten pattern found in iron meteorites of the octahedrite type forms during sub-solidus cooling of metal (Fig. 10). At high temperature ( $> 900$  °C for pure Fe), the stable phase of Fe–Ni alloy is taenite ( $\gamma$ , face centered cubic). As the metal enters the two-phase stability field of taenite + kamacite ( $\alpha$ , body centered cubic), kamacite can nucleate and grow.

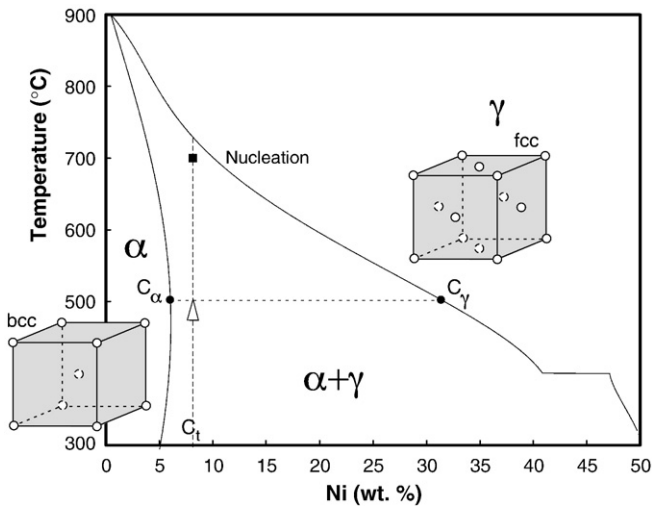


Fig. 10. Fe–Ni phase diagram (P-free system, Hopfe and Goldstein, 2001). The vertical dashed line corresponds to the thermal evolution of bulk Toluca (Ni=8.14 wt.%). Under metastable conditions, kamacite can nucleate after the meteorite enters the 2 phase stability field  $\alpha+\gamma$  (undercooling). At all temperatures, the width of taenite and kamacite can be computed for equilibrium conditions using the lever rule,  $w\alpha/(w\alpha+w\gamma)=(C_t-C_\gamma)/(C_\alpha-C_\gamma)$ . Growth of kamacite is limited by Fe–Ni diffusion in taenite and the actual width of the kamacite crystals is always lower than that given for equilibrium conditions (Wood, 1964; Goldstein and Ogilvie, 1965).

Nickel concentration profiles measured across taenite and kamacite often show gradients as a result of the sub-solidus growth of kamacite out of taenite in diffusion-limited conditions. Wood (1964) and Goldstein and Ogilvie (1965) first analyzed this process quantitatively and showed how measured Ni concentration profiles (e.g., taenite half-width and central Ni concentration) could be used to estimate cooling rates (CR). CR play a central role in meteorite studies because they provide important information on parent body sizes that would be unavailable otherwise (e.g., Chabot and Haack, 2006). Tremendous advances have been made over the past 40 years on the characterization of the Fe–Ni phase diagram, the relevant interdiffusion coefficients, the influence of trace elements, and the treatment of nucleation (Yang and Goldstein, 2006, and references therein). Still, some aspects of the formation of Widmanstätten pattern are not well understood and deserve further investigation. Dauphas (2007) recently showed how Fe and Ni isotopic compositions could be used to test the models of formation of the Widmanstätten pattern directly.

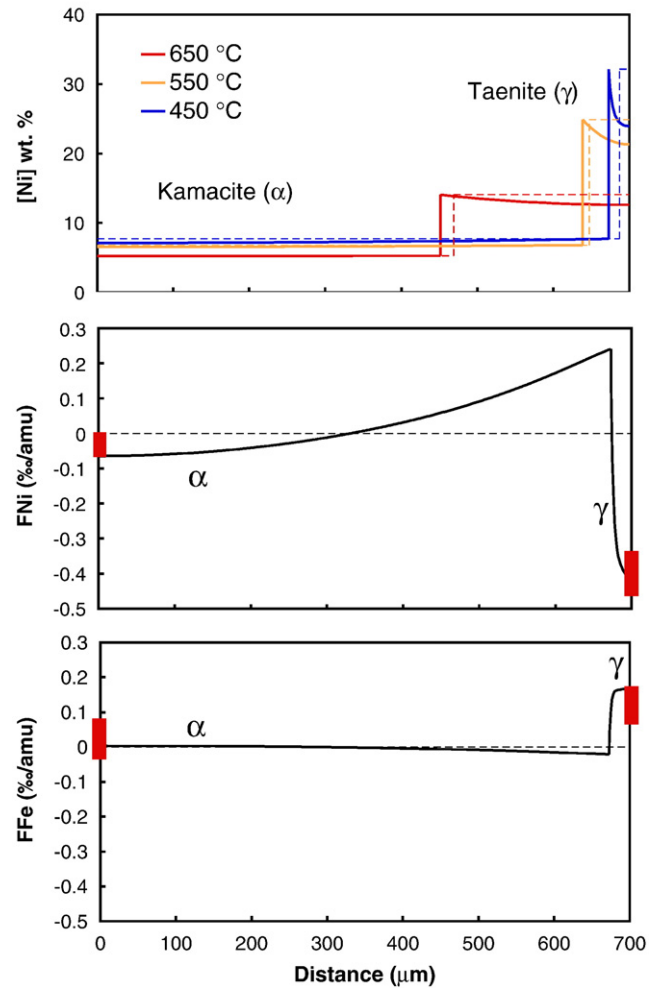
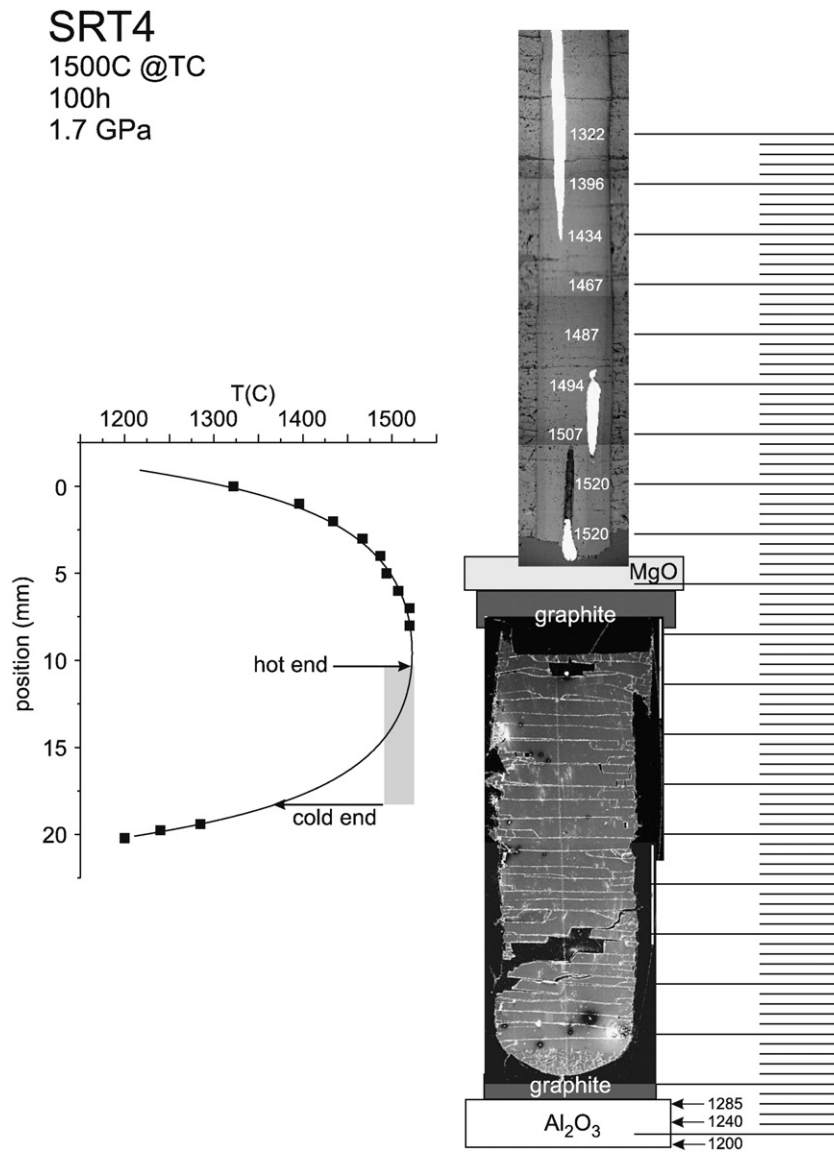


Fig. 11. Modeled Ni concentration (top panel, Hopfe and Goldstein, 2001; Dauphas, 2007) and Ni and Fe isotopic compositions (middle and bottom panels, respectively, Dauphas, 2007) for Toluca IAB iron meteorite and a CR of 50 °C/Myr. In these figures, the center of kamacite is at the left and the center of taenite at the right. Dashed lines correspond to expectations for bulk equilibrium growth conditions (lever rule, Fig. 9). The different curves correspond to snapshots taken at different temperatures during cooling of the meteorite (650, 550, and 450 °C). As is expected, the isotopic fractionations of Fe and Ni go in opposite directions and the magnitude of the fractionation of Ni is larger than that of Fe. The red rectangles are measured Fe and Ni isotopic compositions of taenite and kamacite in Toluca, reported relative to the bulk composition (Poitrasson et al., 2005; Horn et al., 2006; Cook et al., 2007). See Dauphas (2007) for details.

The Toluca (IAB) iron meteorite has been the focus of several studies aimed at measuring Fe and Ni isotopic fractionation between taenite and kamacite (Poitrasson et al., 2005; Horn et al., 2006; Cook et al., 2007). The picture that emerges is that in Toluca, kamacite has heavy Ni isotopic composition (~ + 0.4‰/amu) and light Fe isotopic composition (~ - 0.1‰/amu) relative to taenite. The measurements obtained so far have limited spatial resolution and represent surface averages (spots of 100µm diameter or more). Dauphas (2007) showed that this could be explained by diffusive separation of isotopes during diffusion-limited kamacite growth. Qualitatively, it is easy to understand how diffusion could fractionate isotopes in a manner that can explain the observations made in Toluca. Light isotopes tend to diffuse faster than heavy ones ( $\beta$  is always positive in Fig. 8). Iron meteorites are composed of two major elements, Fe and Ni. The closure condition  $Fe + Ni = 100\%$  implies that the concentration gradients are opposite and therefore that the fluxes of diffusing atoms of Fe and Ni must be

equal in magnitude but opposite in sign ( $\partial Fe/\partial x = -\partial Ni/\partial x$ ). Consequently, one would expect isotopic fractionation of Fe and Ni to go in opposite directions, which is what is observed. The phase diagram of Fe–Ni is such that in both taenite and kamacite, the concentration of Fe is always higher than that of Ni at all temperatures (Fig. 10). The diffusing atoms of iron are mixed with a higher background of normal Fe than in the case of Ni, which explains why the isotopic fractionation of Ni is so much larger than that of Fe.

Dauphas (2007) quantitatively modeled this process of diffusion-driven kinetic isotope fractionation of Fe and Ni associated with growth of kamacite out of taenite during cooling of the Toluca iron meteorite. It is a complex system to model, involving a moving boundary and changing conditions at the interface. Growth of kamacite out of taenite is mainly limited by diffusion in taenite. The phase diagram is such that the Ni concentration in taenite at the interface increases with decreasing temperature. The net Ni flux in



**Fig. 12.** A backscattered electron image of the exposed portion of quenched basalt glass enclosed in graphite recovered from experiment SRT4 is shown on the right. The light colored lines are decompression fractures and at the very bottom end of the sample one can see a small region (~400 µm) where a small amount of olivine crystallized. The scale bar on the right is in mm further subdivided into 200 µm intervals. In the upper part of the picture shows a ground-down portion of the alumina (Al<sub>2</sub>O<sub>3</sub>) tube used to isolate thermocouple wires, which show up as white where exposed. The alumina tube was surrounded by MgO and the temperatures indicated at various points along the alumina tube were determined by the thickness of the spinel layer that formed during the run by the reaction of Al<sub>2</sub>O<sub>3</sub> with MgO (see Watson et al., 2002 for a description of the spinel thermometry method). MgO chips were also placed in contact with the alumina spacer at the bottom of the assembly allowing for a determination of temperature there. The graph on the left shows the temperature determinations together with the position of the molten basalt sample in the temperature profile.

taenite is therefore from the interface toward the center. Because light isotopes tend to diffuse faster than heavy ones, the center of taenite has light Ni isotopic composition relative to the interface and kamacite. As expected, the opposite is true for Fe. The predicted Ni concentration profile and Fe and Ni isotopic compositions for a cooling rate of 50 °C/Myr in the Toluca iron meteorite are compared with actual measurements in Fig. 11. The cooling rate of 50 °C/Myr is much the same as that inferred by the earlier work of Hopfe and Goldstein (2001). The fractionations predicted between taenite and kamacite (around -0.4‰/amu for Ni and +0.2‰/amu for Fe) are very close to the measured compositions in Toluca.

#### 4. Isotope fractionation by thermal (Soret) diffusion in silicate melts

It has been known for quite a long time that a thermal gradient imposed for a sufficiently long time on an initially homogeneous silicate liquid will induce a migration of CaO, MgO, FeO to the cold end while the SiO<sub>2</sub>, Na<sub>2</sub>O, and K<sub>2</sub>O will migrate to the hot end of the temperature gradient (see Bowen, 1921 for an early discussion and Leshner and Walker, 1986 for some excellent experimental results). The realization that isotopes could also be fractionated by a thermal gradient is much more recent. Kyser et al. (1998) showed the unexpected result that oxygen isotopes could become fractionated by several per mil due to an imposed temperature difference of several hundred degrees centigrade across 4 mm of a silicate liquid. These fractionation processes are often referred to as thermal diffusion or Soret diffusion, but these terms are somewhat misleading in the sense that the elemental and isotopic fractionations persist in the steady state after all net chemical transport by diffusion has gone to zero. This is in marked contrast to chemical diffusion effects, which vanish at sufficiently long time. Here we use some of our recent experimental results to illustrate how a temperature gradient across a basalt liquid can fractionate both elements and isotopes.

There are three main differences between the thermal diffusion experiments and those we used to study isotopic fractionation by chemical diffusion between rhyolite-basalt (see Section 3). The most obvious difference is that in the case of the thermal diffusion experiments the entire sample consisted of mid-ocean ridge basalt. Both the chemical and thermal diffusion experiments were run in a piston cylinder apparatus, but for the thermal diffusion experiments the sample was intentionally displaced from the hot spot of the furnace assembly in order that there would be a significant temperature difference across the sample. The final difference is that in the thermal diffusion experiments the temperature at various

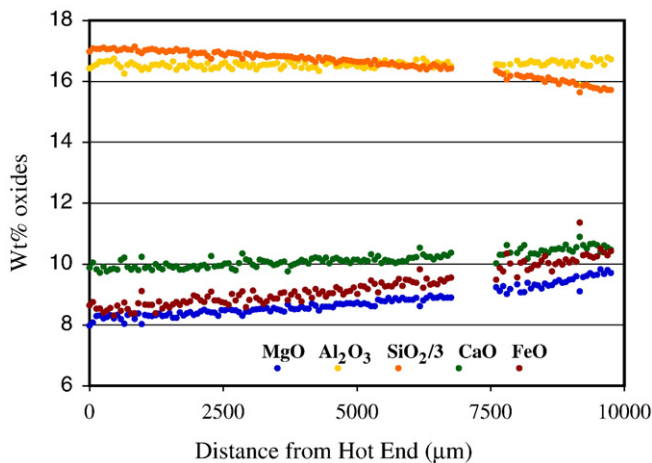


Fig. 13. Weight percent of the various major oxides in the quenched basalt from a thermal diffusion experiment (SRT4 from Richter et al., 2008) with 170 °C across the molten basalt sample (see Fig. 12 for the temperature distribution). The end of the sample that was at the higher temperature is on the left.

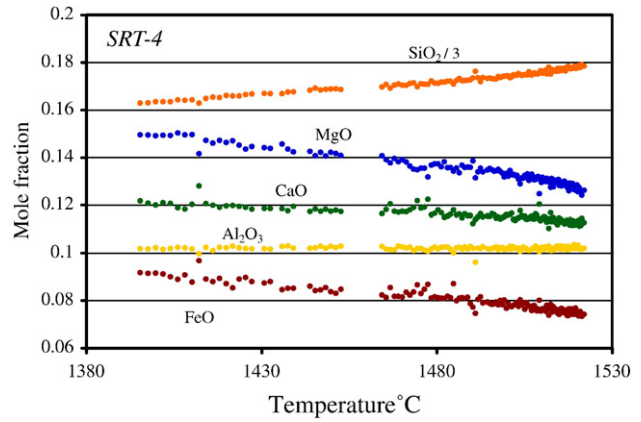


Fig. 14. Mole fraction of the major oxides plotted as a function of temperature. Data from sample SRT4 reported by Richter et al. (2008).

point in the sample assembly was monitored by a method developed by Watson et al. (2002) involving the thickness of a spinel layer that develops wherever Al<sub>2</sub>O<sub>3</sub> is put in contact with MgO. Fig. 12 shows the temperature gradient above and below a typical thermal diffusion sample (SRT4) that was run in a piston cylinder for 100 h at 1.7 GPa. The total temperature difference is about 170 °C.

Fig. 13 shows the weight percent of the various major oxide components as a function of distance from the hot end of sample STR4. As expected the thermal gradient has induced an increase in the weight percent of CaO, MgO, and FeO at the cold end, while the SiO<sub>2</sub> and Na<sub>2</sub>O contents have increased at the hot end. An abrupt change in the weight percent of the various oxides beyond 9500 µm is the result of a small amount of olivine having crystallized there. This region with crystals can also be seen at the bottom of the backscattered image in Fig. 12. We do not think this crystallization will have affected the isotopic fractionations in that, as we noted in Section 1, isotope fractionation associated with olivine crystallizing from a basaltic melt is very small (except possibly for Fe).

Fig. 14 shows the mole fraction of the various oxides plotted as a function of the temperature along the thermal diffusion couple. The gradients in mole fraction with respect to temperature can be used to calculate bulk Soret coefficients, which are the typical way of characterizing

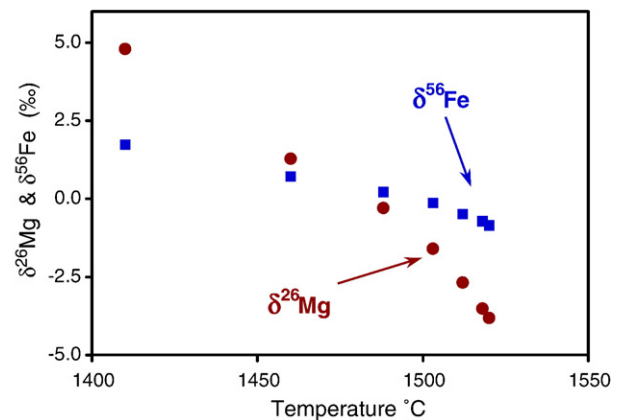


Fig. 15. Magnesium and iron isotopic fractionation as a function of temperature of chips from sample SRT4 reported as

$$\delta^{26}\text{Mg}\text{‰} = 1000 \times \left( \frac{\left( \frac{^{26}\text{Mg}}{^{24}\text{Mg}} \right)_{\text{sample}}}{\left( \frac{^{26}\text{Mg}}{^{24}\text{Mg}} \right)_{\text{bulk-basalt}}} - 1 \right);$$

$$\delta^{56}\text{Fe}\text{‰} = 1000 \times \left( \frac{\left( \frac{^{56}\text{Fe}}{^{54}\text{Fe}} \right)_{\text{sample}}}{\left( \frac{^{56}\text{Fe}}{^{54}\text{Fe}} \right)_{\text{bulk-basalt}}} - 1 \right).$$

how temperature gradients affect chemical composition. The bulk Soret coefficient,  $\sigma_i$ , we use here is that given by [Leshner and Walker \(1986\)](#) as  $\sigma = -\frac{1}{(1-w_i)w_i} dw_i/dT$  where  $w_i$  is the mole fraction of oxide component  $i$  in the bulk composition and  $dw_i/dT$  is the slope of mole fraction/temperature shown in [Fig. 14](#). The Soret coefficients for the major oxides are  $\sigma_{\text{MgO}} = 1.6 \times 10^{-3}$ ,  $\sigma_{\text{CaO}} = 7.0 \times 10^{-4}$ ,  $\sigma_{\text{FeO}} = 1.9 \times 10^{-3}$ ,  $\sigma_{\text{SiO}_2} = -1.5 \times 10^{-3}$ ,  $\sigma_{\text{Al}_2\text{O}_3} \sim 0$ .

A somewhat surprising result is that there are very significant isotopic fractionations due to the temperature difference across the basalt sample SRT4. This is illustrated in [Fig. 15](#) showing magnesium and iron isotope fractionations as a function of temperature from experiment SRT4 of [Richter et al. \(2008\)](#). The isotopic fractionations of magnesium and iron can be fairly described as extraordinarily large by various measures. They are certainly very much larger than our analytical precision which is better than 0.1‰ ( $2\sigma$ ). They are also much larger than the natural variability of the magnesium and iron isotopic composition of igneous rocks, which are at most a few tenths of per mil. Most surprisingly, when isotopic fractionations shown in [Fig. 15](#) are characterized in terms of a thermal isotopic fractionation sensitivity factor  $\Omega$ , defined as the isotopic fractionation in per mil per °C per atomic mass unit, they are comparable or even larger than what has been found in the case of gases. Normally one would expect isotopic fractionation processes to be much more effective in gases compared to that in condensed systems. This is certainly the case for isotopic fractionations by chemical diffusion. However in the case of thermal diffusion we find  $\Omega_{\text{Mg}} = 3.6\text{‰}/^\circ\text{C amu}$  and  $\Omega_{\text{Fe}} = 1.5\text{‰}/^\circ\text{C amu}$  whereas for thermal fractionations of nitrogen  $^{29}\text{N}_2$  versus  $^{28}\text{N}_2$  at temperatures between  $-60^\circ\text{C}$  and  $0^\circ\text{C}$  [Grachev and Severinghaus \(2003\)](#) reported  $\Omega_{\text{N}_2} = 1.5\text{‰}/^\circ\text{C amu}$ . That thermal isotopic fractionations in molten basalt are comparable and sometimes even larger than that in a gas is in our opinion quite remarkable.

## 5. Summary

We have used a variety of laboratory and field data to illustrate high temperature isotopic fractionations by processes such as evaporation, chemical diffusion, and thermal (Soret) diffusion. Of these various processes, kinetic isotope fractionation by evaporation is the most extensively studied in terms of its use to constrain the thermal processing of a natural material as in the case of calcium–aluminum-rich inclusions (CAIs) in chondritic meteorites. The correlated enrichment of CAIs in the heavy isotopes of Si and Mg is almost perfectly reproduced by laboratory experiments and there is little doubt that the isotopic fractionations of the CAIs are the result of evaporation while they were partially molten. The laboratory determinations of the kinetic isotope fractionation factors for evaporation of silicon and magnesium from a silicate liquid (i.e., the  $\alpha$  exponent in a Rayleigh fractionation equation) can then be used to determine the fraction of Si and Mg that was evaporated. Combining the amount of these volatile elements that was evaporated with laboratory determined evaporation rates imposes quantitative constraints on the duration of the high temperature evaporation event.

The use of kinetic isotope fractionations by chemical diffusion to interpret the evolution of natural systems is far less mature than in the case of evaporation, but there are various lines of evidence showing that these processes do occur and leave a measurable isotopic fractionation. The two natural examples we discussed here involved the isotopic fractionation of Li as it diffused from a pegmatite into the surrounding country rock and the fractionation of Fe and Ni isotopes during their interdiffusion in a cooling Fe–Ni meteorite.

In connection with thermal fractionation of elements and isotopes we should acknowledge and address [Bowen \(1921\)](#) contention that such thermal processes are of little practical interest for igneous petrology. His argument is based on the fact that thermal diffusion in melts is many orders magnitude faster than chemical diffusion and thus thermal gradients would dissipate much too fast for very much

chemical (or isotopic) fractionation to have taken place. This will certainly be true in most circumstances affecting igneous rocks, but not necessarily all circumstances. The most likely exception will be in thermal boundary layers of molten silicate systems where the temperature and crystal fraction dependence of the viscosity can result in a stagnant layer where temperature gradients are maintained by flow at the interior edge of the boundary layer. An example of this might be found in the case of basaltic dykes where the flow of hot basalt in the core of a propagating dyke will maintain a temperature gradient from core to edge for times much larger than one would calculate based on the diffusion time scale. A diagnostic fingerprint of Soret diffusion is the presence of positively correlated Fe and Mg isotopic fractionations.

## Acknowledgments

This work was supported by the France–Chicago Center, a Packard fellowship and the National Aeronautics and Space Administration through grant NNG06GG75G (to N.D.), and DOE grant (DE-FG02-01ER15254,A005) and NASA (NNG06GE85G) grants to FMR.

## References

- Aulbach, S., Rudnick, R.L., McDonough, W.L., 2008. Li–Sr–Nd isotope signatures of the plume and cratonic lithospheric mantle beneath the margin of the rifted Tanzanian craton (Labait). *Contrib. Mineral. Petrol.*, 155, 79–92.
- Alexander, C.M.O'D., Hewins, R.H., 2004. Mass fractionation of Fe and Ni isotopes in metal in Hammadah Al Hamrah. *Annual Meteoritical Society Meeting 67* #5080.
- Bartdorff, D., Reimers, P., 1975. The isotope effect of silver diffusion in aluminum. *Phys. Status Solidi* 28, 433–438.
- Batra, A.P., 1967. Anisotropic isotope effect for diffusion of zinc and cadmium in zinc. *Phys. Rev.* 159, 487–499.
- Beck, P., Chaussidon, M., Barrat, J.A., Gillet, P., Bohn, M., 2006. Diffusion induced Li isotopic fractionation during the cooling of magmatic rocks: the case of pyroxene phenocrysts from nakhlite meteorites. *Geochim. Cosmochim. Acta* 70 (18), 4813–4825.
- Bharati, S., Sinha, A.P.B., 1977. Isotope effect and correlation factor for the diffusion of cadmium in silver. *Phys. Status Solidi* 44, 391–399.
- Bigeleisen, J., Mayer, M.G., 1947. Calculation of equilibrium constants for isotopic exchange reactions. *J. Chem. Phys.* 15 (5), 261–267.
- Bowen, N.L., 1921. Diffusion in silicate melts. *J. Geol.* 29, 295–317.
- Bussmann, W., Herzig, C., Hoff, H.A., Mundy, J.N., 1981. Isotope effect in niobium self-diffusion. *Phys. Rev. B* 23, 6216–6222.
- Bussmann, W., Herzig, C., Rempp, W., Maier, K., Mehrer, H., 1979. Isotope effect and self-diffusion in face-centred cubic cobalt. *Phys. Status Solidi* 56, 87–97.
- Campbell, D.R., 1975. Isotope effect for self-diffusion in Ge. *Phys. Rev. B* 12, 2318–2322.
- Chabot, N.L., Haack, H., 2006. Evolution of asteroidal cores. In: Lauretta, D.S., McSween, H.Y., Tucson (Eds.), *Meteorites and the Early Solar System II*. The University of Arizona Press, Arizona, pp. 747–771.
- Chan, L.H., Edmond, J.M., Thompson, G., Gillis, K., 1992. Lithium isotopic composition of submarine basalts: implications for the lithium cycle in the oceans. *Earth Planet. Sci. Lett.* 108 (1–3), 151–160.
- Coleman, M.G., Wert, C.A., Peart, R.F., 1968. Isotope effect for diffusion of iron in vanadium. *Phys. Rev.* 175, 788–795.
- Coogan, L.A., Kasemann, S.A., Chakraborty, S., 2005. Rates of hydrothermal cooling of new oceanic upper crust derived from lithium–geospeedometry. *Earth Planet. Sci. Lett.* 240 (2), 415–424.
- Cook, D.L., Wadhwa, M., Clayton, R.N., Dauphas, N., Janney, P.E., Davis, A.M., 2007. Mass-dependent fractionation of nickel isotopes in meteoritic metal. *Meteoritics Planet. Sci.*, 42, 2067–2077.
- Dauphas, N., Janney, P.E., Mendybaev, R.A., Wadhwa, M., Richter, F.M., Davis, A.M., van Zuilen, A., Hines, R., Foley, C.N., 2004. Chromatographic separation and multi-collection-ICPMS analysis of iron. Investigating mass-dependent and -independent isotope effects. *Anal. Chem.* 76, 5855–5863.
- Dauphas, N., 2007. Diffusion-driven kinetic isotope effect of Fe and Ni during formation of the Widmanstätten pattern. *Meteoritics Planet. Sci.* 42, 1597–1614.
- Davis, A.M., Hashimoto, A., Clayton, R.N., Mayeda, T.K., 1990. Isotope mass fractionation during evaporation of forsterite ( $\text{Mg}_2\text{SiO}_4$ ). *Nature* 347, 655–658.
- Davis, A.M. and Richter, F.M., 2004. Condensation and evaporation of solar system materials, pp. 407–430. In *Meteorites, Comets, and Planets* (ed. A.M. Davis.) Vol 1. *Treatise on Geochemistry* (eds. H.D. Holland and K.K. Turekian), Elsevier–Pergamon, Oxford.
- Ecksele, H., Herzig, C., 1978. On the mass dependence of the energy factor DK of the isotope effect for impurity diffusion in copper. *Phys. Status Solidi* 85, 185–193.
- Fishman, S.G., Gupta, D., Lieberman, D.S., 1970. Diffusivity and isotope-effect measurements in equiatomic Fe–Co. *Phys. Rev. B* 2, 1451–1460.
- Gibbs, G.B., Graham, D., Tomlin, D.H., 1963. Diffusion in titanium and titanium–niobium alloys. *Phil. Mag.* 8, 1269–1282.
- Giletti, B.J., Shanahan, T.M., 1997. Alkali diffusion in plagioclase feldspar. *Chem. Geol.* 139 (1–4), 3–20.

- Goldstein, J.I., Ogilvie, R.E., 1965. The growth of the Widmanstätten pattern in metallic meteorites. *Geochim. Cosmochim. Acta* 29, 893–920.
- Grachev, A.M., Severinghaus, J.P., 2003. Laboratory determination of thermal diffusion constants for  $^{29}\text{N}_2/^{28}\text{N}_2$  in air at temperatures from -60 to 0 °C for reconstruction of the magnitudes of abrupt climate changes using the ice core fossil-air paleothermometer. *Geochim. Cosmochim. Acta* 67, 345–360.
- Graham, D., 1969. Mass dependence of self-diffusion in iron. *J. Appl. Phys.* 40, 2386–2390.
- Halama, R., McDonough, W.F., Rudnick, R.L., Keller, J., Klaudius, J., 2007. The Li isotopic composition of Oldoinyo Lengai: nature of the mantle sources and lack of isotopic fractionation during carbonatite petrogenesis. *Earth Planet. Sci. Lett.* 254 (1–2), 77–89.
- Hashimoto, A., 1990. Evaporation kinetics of forsterite and implications for the early solar nebula. *Nature* 347, 53–55.
- Hehenkamp, T., Lodding, A., Odelius, H., Schlett, V., 1979. Isotope effect in the diffusion of the stable germanium isotopes in copper. *Acta Metall.* 27, 829–832.
- Hehenkamp, T., Schlett, V., 1977. Isotope effect for diffusion of germanium in copper-germanium solid solutions. *Acta Metall.* 25, 110–114.
- Helz, R.T., 1987. Differentiation behavior of Kilauea Iki lava lake, Kilauea Volcano, Hawaii: An overview of past and current work. In: Mysen, B.O. (Ed.), *Magmatic Processes: Physicochemical Principles*. Geochim. Soc. Spec. Publ., 1, pp. 241–258.
- Herzig, C., Eckseler, H., Bussmann, W., Cardis, D., 1978. The temperature dependence of the isotope effect for self-diffusion and cobalt impurity-diffusion in gold. *J. Nucl. Mater.* 69–70, 61–69.
- Heumann, T., Imm, R., 1968. Self-diffusion and isotope effect in g-iron. *J. Phys. Chem. Solids* 29, 1613–1621.
- Heumann, T., Kohl, J.G., 1974. Der Isotopieeffekt bei der diffusion von magnesium in solber. *Massenspektrometrische methode*. *Acta Metall.* 22, 21–26.
- Hirth, J.P., Pound, G.M., 1963. *Condensation and evaporation nucleation and growth kinetics*. Macmillan, New York. 191 pp.
- Hopfe, W.D., Goldstein, J.I., 2001. The metallographic cooling rate method revised: application to iron meteorites and mesosiderites. *Meteoritics Planet. Sci.* 36, 135–154.
- Horn, I., Von Blanckenburg, F., Schoenberg, R., Steinhofel, G., Markl, G., 2006. In situ iron isotope ratio determination using UV-femtosecond laser ablation with application to hydrothermal ore formation processes. *Geochim. Cosmochim. Acta* 70, 3677–3688.
- Iijima, Y., Kimura, K., Hirano, K., 1988. Self-diffusion and isotope effect in a-iron. *Acta Metall.* 36, 2811–2820.
- Irmer, V., Feller-Kniepmeier, M., 1972. Isotope effect for self-diffusion in single crystals of a iron and correlation factor of solute diffusion in a iron. *J. Appl. Phys.* 43, 953–957.
- Jackson, M.S., Lazarus, D., 1977. Isotope effect for diffusion of tin in b-titanium. *Phys. Rev. B* 15, 4644–4656.
- Janney, P.E., Richter, F.M., Davis, A.M., Mendybaev, R.A., Wadhwa, M., 2005. Silicon Isotope Ratio Variations in CAI Evaporation Residues Measured by Laser Ablation. *Lunar and Planetary Science XXXVI*, Abstract #2123, Lunar and Planetary Institute, Houston. (CD-ROM).
- Jeffcoate, A., et al., 2007. Li isotope fractionation in peridotites and mafic melts. *Geochim. Cosmochim. Acta*, 71, 202–218.
- Kyser, T.K., Leshner, C.E., Walker, D., 1998. The effects of liquid immiscibility and thermal diffusion on oxygen isotopes in silicate liquids. *Contrib. Mineral. Petrol.* 133, 373–381.
- LeClaire, A.D., Lidiard, A.B., 1956. LIII. Correlation effects in diffusion in crystals. *Phil. Mag.* 1, 518–527.
- Leshner, C.E., Walker, D., 1986. Solution properties of silicate liquids from thermal diffusion experiments. *Geochim. Cosmochim. Acta* 50, 1397–1411.
- Lundstrom, C.C., Chaussidon, M., Hsu, A.T., Kelemen, P., Zimmerman, M., 2005. Observations of Li isotopic variations in the Trinity Ophiolite: evidence for isotopic fractionation by diffusion during mantle melting. *Geochim. Cosmochim. Acta*, 69 (3), 735–751.
- Mali, M., Roos, J., Sonderegger, M., Brinkmann, D., Heitjans, P., 1988.  $^6\text{Li}$  and  $^7\text{Li}$  diffusion coefficients in solid lithium measured by the NMR pulsed field gradient technique. *J. Phys. F: Met. Phys.* 18, 403–412.
- Manke, L., Herzig, C., 1982. Diffusion und Isotopieeffekt von silber in b-zircon. *Acta Metall.* 30, 2085–2092.
- Marks, M.A.W., Rudnick, R.L., McCammon, C., Vennemann, T., Markl, G., 2007. rrested kinetic Li isotope fractionation at the margin of the Ilimaussaq complex, South Greenland: Evidence for open-system processes during final cooling of peralkaline igneous rocks. *Chemical Geology*. doi:10.1016/j.chemgeo.2007.10.001.
- McCracken, G.M., Love, H.M., 1960. Diffusion of lithium through tungsten. *Phys. Rev. Lett.* 5, 201–202.
- Miller, J.W., Edelstein, W.A., 1969. Isotope effect for the diffusion of cadmium in lead. *Phys. Rev.* 188, 1081–1088.
- Mullen, J.G., 1961. Isotope effect in intermetallic diffusion. *Phys. Rev.* 121, 1649–1658.
- Mundy, J.N., 1971. Effect of pressure on the isotope effect in sodium self-diffusion. *Phys. Rev. B* 3, 2431–2445.
- Mundy, J.N., McFall, W.D., 1973. Comparison of the isotope effect for diffusion of sodium and silver in lithium. *Phys. Rev. B* 7, 4363–4370.
- Mundy, J.N., Miller, J.W., Rothman, S.J., 1974. Diffusion of copper in lead: solubility and isotope effect. *Phys. Rev. B* 10, 2275–2280.
- Mundy, J.N., Tse, C.W., McFall, W.D., 1976. Isotope effect in chromium self-diffusion. *Phys. Rev. B* 13, 2349–2357.
- Nichols, R.H., Grimley, R.T., Wasserburg, G.J., 1998. Measurement of gas-phase species during Langmuir evaporation of forsterite. *Meteorit. Planet. Sci.* 33 A115.
- Oviedo de Gonzalez, C., Walsoe de Reza, N.E., 1971. Isotope effect in iron diffusion in Fe/3% Si alloy. *J. Phys. Chem. Solids* 32, 1067–1074.
- Pell, E.M., 1960. Diffusion of Li in Si at high T and the isotope effect. *Phys. Rev.* 119, 1014–1021.
- Peterson, N.L., 1964. Isotope effect in self-diffusion in palladium. *Phys. Rev.* 136, A568–A574.
- Peterson, N.L., Rothman, S.J., 1967. Isotope effect for the diffusion of zinc in copper, and ordered and disordered CuZn. *Phys. Rev.* 154, 558–560.
- Peterson, N.L., Rothman, S.J., 1967. Isotope effect in self-diffusion in zinc. *Phys. Rev.* 163, 645–649.
- Peterson, N.L., Rothman, S.J., 1970. Diffusion and correlation effects in copper-zinc alloys. *Phys. Rev. B* 2, 1540–1547.
- Peterson, N.L., Rothman, S.J., 1978. Isotope effect for diffusion of zinc and copper in aluminum. *Phys. Rev. B* 17, 4666–4673.
- Poitrasson, F., Levasseur, S., Teutsch, N., 2005. Significance of iron isotope mineral fractionation in pallasites and iron meteorites for the core-mantle differentiation of terrestrial planets. *Earth Planet. Sci. Lett.* 234, 151–164.
- Richter, F.M., Liang, Y., Davis, A.M., 1999. Isotope fractionation by diffusion in molten oxides. *Geochim. Cosmochim. Acta* 63, 2853–2861.
- Richter, F.M., Davis, A.M., DePaolo, D.J., Watson, E.B., 2003. Isotope fractionation by chemical diffusion between molten basalt and rhyolite. *Geochim. Cosmochim. Acta* 67, 3905–3923.
- Richter, F.M., 2004. Timescales determining the degree of kinetic isotope fractionation by evaporation and condensation. *Geochim. Cosmochim. Acta* 68, 4971–4992.
- Richter, F.M., Mendybaev, R.A., Davis, A.M., 2006a. Conditions in the protoplanetary disk as seen by refractory inclusions in meteorites. *Meteorit. Planet. Sci.* 41, 83–93.
- Richter, F.M., Mendybaev, R.A., Christensen, J.N., Hutcheon, I.D., Williams, R.W., Sturchio, N.C., Beloso Jr., A.D., 2006b. Kinetic isotope fractionation during diffusion of ionic species in water. *Geochim. Cosmochim. Acta* 70, 277–289.
- Richter, F.M., Janney, P.E., Mendybaev, R.A., Davis, A.M., Wadhwa, M., 2007. Elemental and isotopic fractionation of Type B CAI-like liquids by evaporation. *Geochim. Cosmochim. Acta*, 71, 5544–5564.
- Richter, F.M., Watson, E.B., Mendybaev, R.A., Teng, F.-Z., Janney, P.E., 2008. Magnesium isotope fractionation in silicate melts by chemical and thermal diffusion. *Geochim. Cosmochim. Acta* 72, 206–220.
- Rockosch, H.-J., Herzig, C., 1983. Isotope effect of manganese and simultaneous impurity diffusion of chromium and zinc in copper. *Phys. Status Solidi* 119, 199–207.
- Rockosch, H.-J., Herzig, C., 1984. Isotope effect of impurity diffusion of cadmium in silver. *Acta Metall.* 32, 503–509.
- Rodushkin, I., Stenberg, A., Andrén, H., Malinovsky, D., Baxter, D.C., 2004. Isotopic fractionation during diffusion of transition metal ions in solution. *Anal. Chem.* 76, 2148–2151.
- Roskosz, M., Luais, B., Watson, H.C., Toplis, M.J., Alexander, C.M.o'D., Mysen, B.O., 2006. Experimental quantification of the fractionation of Fe isotopes during metal segregation from a silicate melt. *Earth Planet. Sci. Lett.* 248, 851–867.
- Rothman, S.J., Peterson, N.L., 1967. Correlation coefficient and the isotope effect for the diffusion of zinc in silver. *Phys. Rev.* 154, 552–558.
- Rothman, S.J., Peterson, N.L., Robinson, J.T., 1970. Isotope effect for self-diffusion in single crystals of silver. *Phys. Status Solidi* 39, 636–645.
- Rudnick, R.L., Ionov, D.A., 2007. Lithium elemental and isotopic disequilibrium in minerals from peridotite xenoliths from far-east Russia: product of recent melt/fluid-rock interaction. *Earth Planet. Sci. Lett.* 256, 278–293.
- Rudnick, R.L., Tomasacsk, P.B., Njo, H.B., Gardner, L.R., 2004. Extreme lithium isotopic fractionation during continental weathering revealed in sapolites from South Carolina. *Chem. Geol.* 212 (1–2), 45–57.
- Schoen, A.H., 1958. Correlation and the isotope effect for diffusion in crystalline solids. *Phys. Rev. Lett.* 1, 138–140.
- Shi, J., Healy, R.J., Huntington, H.B., 1994. Isotope effect for diffusion of gold in lead-indium alloys. *J. Phys. Chem. Solids* 55, 487–491.
- Stolper, E., Paque, J.M., 1986. Crystallization sequences of Ca–Al-rich inclusions from Allende: the effects of cooling rate and maximum temperature. *Geochim. Cosmochim. Acta* 50, 1785–1806.
- Tang, Y.-J., Zhang, H.-F., Nakamura, E., Moriguti, T., Ying, J.-F., 2007. Lithium isotopic systematics of peridotite xenoliths from Hannuoba, North China Craton: implications for melt–rock interaction in the considerably thinned lithospheric mantle. *Geochim. Cosmochim. Acta* 71 (17), 4327–4341.
- Teng, F.-Z., et al., 2004. Lithium isotopic composition and concentration of the upper continental crust. *Geochim. Cosmochim. Acta* 68 (20), 4167–4178.
- Teng, F.-Z., McDonough, W.F., Rudnick, R.L., Walker, R.J., 2006a. Diffusion-driven extreme lithium isotopic fractionation in country rocks of the Tin Mountain pegmatite. *Earth Planet. Sci. Lett.*, 243 (3–4), 701–710.
- Teng, F.-Z., McDonough, W.F., Rudnick, R.L., Walker, R.J., Sibrescu, M.L.C., 2006b. Lithium isotopic systematics of granites and pegmatites from the Black Hills, South Dakota. *Am. Miner.* 91, 1488–1498.
- Teng, F.-Z., Wadhwa, M., Helz, R.T., 2007. Investigation of magnesium isotope fractionation during basalt differentiation: Implications for a chondritic composition of the terrestrial mantle. *Earth Planet. Sci. Lett.* 261 (1–2), 84–92.
- Teng, F.-Z., Dauphas, N., Helz, R.T., 2008a. Iron isotope fractionation during magmatic differentiation in Kilauea Iki lava lake. *Science in revision*.
- Teng, F.-Z., Rudnick, R.L., McDonough, W.F., Gao, S., Tomasacsk, P.B., Liu, Y., 2008b. Lithium isotopic composition and concentration of the deep continental crust. *Chem. Geol. in revision*.
- Tomasacsk, P.B., Tera, F., Helz, R.T., Walker, R.J., 1999. The absence of lithium isotope fractionation during basalt differentiation: New measurements by multicollector sector ICP-MS. *Geochim. Cosmochim. Acta* 63 (6), 907–910.
- Tothman, S.J., Peterson, N.L., 1969. Isotope effect and divacancies for self-diffusion in copper. *Phys. Stat. Sol.* 35, 205–312.
- Urey, H.C., 1947. The thermodynamic properties of isotopic substances. *J. Chem. Soc. (London)* 562–581.

- Walker, R.J., Hanson, G.N., Papike, J.J., O'Neil, J.R., Laul, J.C., 1986. Internal evolution of the Tin Mountain pegmatite, Black Hills, South Dakota. *Am. Miner.* 71, 440–449.
- Walter, C.M., Peterson, N.L., 1969. Isotope effect in self-diffusion in iron. *Phys. Rev.* 178, 922–929.
- Watson, E.B., Wark, D.A., Price, J.D., Van Orman, J.A., 2002. Mapping the thermal structure of solid-media pressure assemblies. *Contrib. Mineral. Petrol.* 142, 640–652.
- Wood, J.A., 1964. The cooling rates and parent planets of several iron meteorites. *Icarus* 3, 429–459.
- Yang, J., Goldstein, J.I., 2006. Metallographic cooling rates of the IIIAB iron meteorites. *Geochim. Cosmochim. Acta* 70, 3197–3215.
- Zipfel, J., Weyer, S., 2007. In situ analyses of Fe isotopes in zoned metal grains of Hammadad Al Hamra 237. *Lunar Planet. Sci XXXVIII*, #1927.